Received 16 December 2019; accepted 5 March 2020. Date of publication 18 March 2020;
date of current version 1 June 2020. The review of this article was arranged by Associate Editor Xinge Yu.

Digital Object Identifier 10.1109/OJNANO.2020.2981824

Ultrasound Imaging and Tracking of Micro/Nanorobots: From Individual to Collectives

QIANQIAN WANG [1] (Student Member, IEEE), AND LI ZHANG [1–4] (Senior Member, IEEE)

[1]Department of Mechanical and Automation Engineering, The Chinese University of Hong Kong, 999077 Hong Kong, China
[2]Chow Yuk Ho Technology Centre for Innovative Medicine, The Chinese University of Hong Kong, 999077 Hong Kong, China
[3]CUHK T Stone Robotics Institute, The Chinese University of Hong Kong, 999077 Hong Kong, China
[4]Shenzhen Research Institute, The Chinese University of Hong Kong, Shenzhen, China

CORRESPONDING AUTHOR: LI ZHANG (e-mail: lizhang@cuhk.edu.hk)

The work was supported by the Hong Kong Research Grants Council (RGC) with Project Nos. GRF14218516 and JLFS/E- 402/18, the ITF projects with Project Nos. ITS/231/15, MRP/036/18X, and ITS/374/18FP funded by the HKSAR Innovation and Technology Commission (ITC), the Research Sustainability of Major RGC Funding Schemes (RSFS), the Impact Postdoctoral Fellowship Scheme, and the Direct Grant from The Chinese University of Hong Kong.

ABSTRACT The rapid development of untethered micro/nanorobots enables them to be applied in biomedical tasks, such as targeted delivery, localized diagnostics, and minimally invasive surgery. However, many challenges remain before applying these tiny machines to perform therapeutics and intervention in a living body. Among them, one critical issue is the integration of medical imaging systems with micro/nanorobotics to acquire precise feedback *in vivo*. Ultrasound imaging, as one of the widely used mature imaging technologies, shows great potential for providing real-time feedback of micro/nanorobots in 2-D and 3-D space. In this mini-review, the recent progress and challenges on the imaging and tracking of micro/nanorobots using established medical ultrasound imaging technologies are surveyed and summarized. The limitations together with future research opportunities in the real-time navigation of micro/nanorobots *in vivo* and their collectives are discussed.

INDEX TERMS Medical micro/nanorobots, ultrasound imaging, *in vivo* tracking, collective behaviors, real-time feedback control.

I. INTRODUCTION

Micro/nanorobots are untethered small-scale machines capable of navigating in a controlled manner through various physiological environments by external power sources [1]–[11], self-propulsion [12]–[17], and hybrid propulsion [18]–[24]. Recent achievements on the fabrication, actuation, functionalization provide more biocompatible and biodegradable micro/nanorobots with diverse capabilities [25]–[29]. These micro- and nano-scale robots offer potential for diverse biomedical applications such as targeted delivery [30]–[36], biosensing [37]–[41], micromanipulation [42]–[44], and minimally invasive surgery [45]–[48]. Although most of the proof-of-concept applications of micro/nanorobots were demonstrated *in vitro* and *ex vivo*, recent studies have reported that the controllable micro- /nano-agents can be applied *in vivo* via animal tests [49]–[52]. To translate the micro/nanorobotics to clinical applications, one of the indispensable challenge is *in vivo* imaging and tracking of these tiny actuated machines [53], [54].

The effective actuation and visual servoing of micro/nanorobots in a living body require real-time localization. To date, a variety of imaging technologies have been explored for localization of micro/nanorobots, including ultrasound (US) imaging, fluorescent imaging (FI), magnetic resonance imaging (MRI), computed tomography (CT), positron emission tomography (PET), photoacoustic (PA) imaging and single-photon emission computed tomography (SPECT). The position feedback provided by these imaging systems has been applied to close control loops and establish autonomous actuation systems. Among these imaging technologies, US imaging is a widely-used, well-established, radiation-free medical imaging technique. It has been applied in clinical diagnostics,

such as measuring of blood flow and monitoring the fetus in uterus, in the field of pelvis, cardiology, ophthalmology, and orthopedics [55]–[58]. It is based on the reflected acoustic waves that have interacted with the imaging objects and their surrounding environments. Comparing to other medical imaging technologies (e.g., MRI, CT), US imaging provides high temporal resolution (fast imaging speed), which is essential for acquiring real-time feedback of moving objects. Autonomous control loop can be closed with US feedback to perform real-time visual servoing of micro/nanorobots, targeted delivery, and localized therapy. Moreover, the various US imaging modes (e.g., B-mode, Doppler-mode) provide the potential for applying micro/nanorobots to perform demanded tasks in different environments.

US imaging relies on gradients of acoustic impedance, thus the scale of an object should be larger than the sonographic detection limit. One major challenge of using US as the tracking tool is the small size of micro/nanorobots (e.g., sub-millimeter scale). To achieve effective localization and tracking, recent work on collective behaviors of active matter inspires the researchers in introducing swarming micro/nanorobots to achieve imaging-guided delivery. A swarm pattern is formed by gathering the building blocks together, which is usually realized by inducing interactions between these small-scale blocks [59]–[63]. Compared to the usage of a single object, swarming patterns could enhance imaging contrast by increasing the density of the building blocks (micro/nanorobots), thus enabling deep-tissue imaging. The integration of swarm control and US imaging systems will be introduced in this mini-review.

In this mini-review, we summarize the recent progress on the imaging and tracking of micro/nanorobots using established medical US imaging technologies. Recent research efforts in the design, actuation, and control of micro/nanorobots under ultrasound guidance are reviewed. Beside the summary of classic works in US-guided control of individual small-scale robots, the design of swarming micro/nanorobots towards *in vivo* US imaging-guided delivery are summarized. Advantages and limitations of using individual microrobot and swarming microrobots under different US imaging modes are compared. The challenges in real-time navigation of micro/nanorobots *in vivo* and the integration between imaging and control systems are listed and discussed. We end the report with conclusions and some prospective directions.

II. ULTRASOUND IMAGING TECHNOLOGY FOR TRACKING OF MICRO/NANOROBOTS

A. ACTUATED MICROROBOT UNDER ULTRASOUND IMAGING GUIDANCE

One of the commonly-used imaging modes in both clinic and research trials is the B-mode (brightness mode). The greyscale images are acquired through transmission into objects of short ultrasound pulses and recording of backscattered echoes. Because the attenuation and resolution increase with frequency, there is an inherent trade-off between resolution and imaging depth. High-frequency ultrasound waves (e.g., 10–15 MHz) generate images with higher resolution, which can only be used for objects located at a superficial level, such as musculoskeletal imaging and thyroid. Low-frequency waves (e.g., 2–5 MHz) are more suitable for an object located at a deeper place, such as deep abdomen, obstetric and gynecological imaging.

To date, several researchers have proposed strategies of using B-mode US feedback for localization of miniature robots. Misra *et al.* demonstrated a wireless magnetic-based motion control of paramagnetic microparticles under US guidance [64]. The microparticle has a diameter of 100 μm, and it was actuated using magnetic field gradient. The US images provided real-time position of the microparticles, then the tracked position was applied in the implementation of a proportional-derivative magnetic-based control system (Fig. 1(A)). The system achieved point-to-point control of the microparticles with an average position tracking error of 48 $\pm$ 59 μm. As a comparison, such average position tracking reached 21 $\pm$ 26 μm based on a microscopic system. Using the US feedback-integrated control scheme, the microparticles followed different planned trajectories with an average velocity of 94–279 μm/s. To perform manipulation tasks in tortuous environments where traditional microscope cannot reach, Misra and co-workers demonstrated the real-time navigation of a miniature soft gripper [65]. The hydrogel thermal-responsive gripper exhibited fold-unfold transitions by changing the temperature, and the diameter of the gripper was changed from 2 mm to 5 mm. The embedded Fe_2O_3 provides the magnetism so that the gripper can be pulled using magnetic field gradient. A real-time control system was designed based on the feedback from US B-mode images. The gripper was navigated along a sinusoidal planned path at an average speed of 0.41 $\pm$ 0.14 mm/s, where the tracked position from US images is compared with the reference position (Fig. 1(B)). Experimental results showed that the average positioning error is 0.48 $\pm$ 0.1 mm ($\sim$ 12% of the body length of the miniaturized gripper). Such path-following control has been integrated with the ability of obstacle avoidance, where the generated path could avoid virtual obstacles with a safe distance. Moreover, this miniaturized gripper showed the ability to pick-and-place a microbead to a target position. Results showed that the US feedback-based control system has an average tracking error of 0.4 $\pm$ 0.13 mm without payload and 0.36 $\pm$ 0.05 mm when performing a transportation task with a payload. The integration of US imaging and magnetic control system demonstrated the ability to control a miniaturized robot to perform targeted delivery in situations where visual feedback cannot be provided via cameras.

US imaging-guided microrobots have also been investigated toward medical applications. Recently, Khalil *et al.* proposed the mechanical rubbing of blood clots using a US-guided magnetic helical miniature robot *ex vivo* [66]. The helical robot has the diameter and length of around 1 mm $\times$ 8 mm. US feedback provided the position of the robot in real time, which was used to control its motion toward

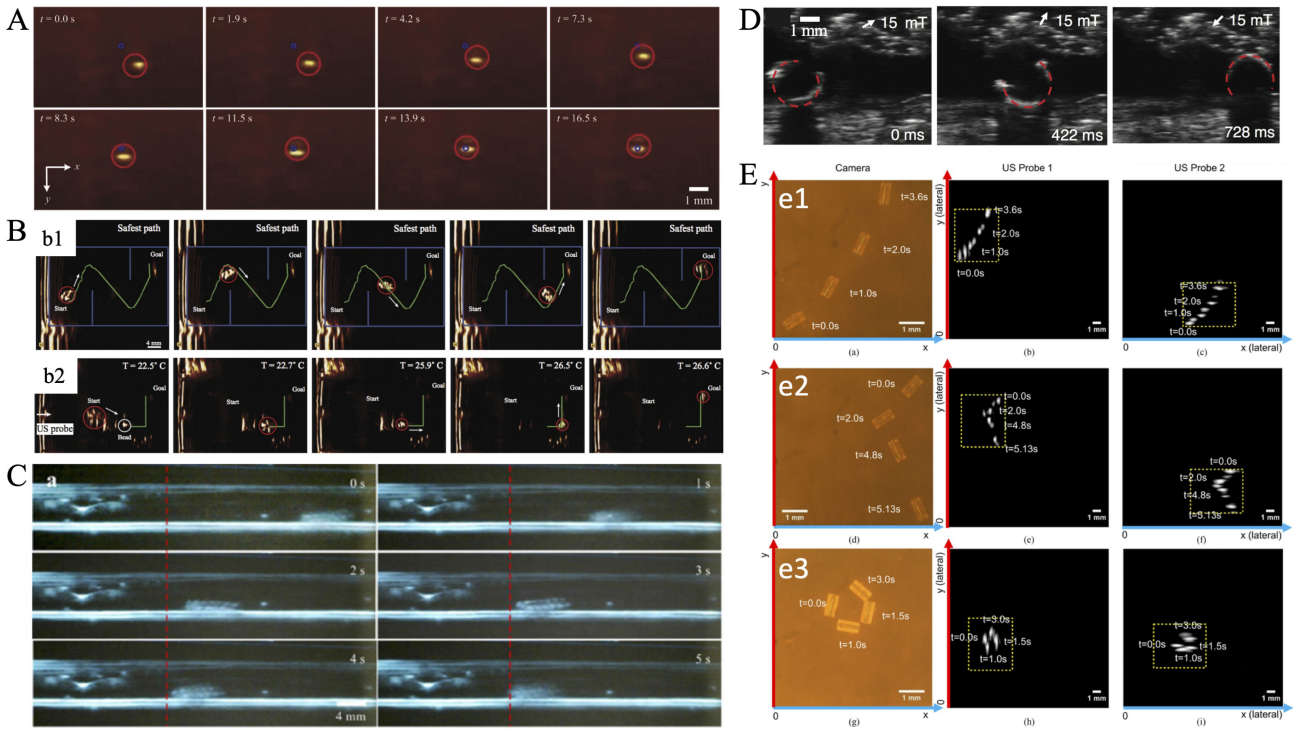

FIGURE 1. **Localization of an individual microrobot under B-mode US imaging. (A) Closed-loop control of a paramagnetic microparticle using US feedback [64]. Reproduced with permission. Copyright 2014, IEEE. (B) Magnetic motion control and path planning of an untethered gripper. The gripper was navigated along the planned path with (b1) obstacle-avoidance ability and (b2) thermally controlled deformation [65]. Reproduced with permission. Copyright 2017, IEEE. (C) Closed-loop control of a helical millimeter-size robot for thrombolysis using US feedback [66]. Reproduced with permission. Copyright 2017, IEEE. (D) US-guided locomotion of a soft miniature robot. The robot rolls within a tube embedded in an *ex vivo* chicken tissue [67]. Reproduced with permission. Springer Nature, 2018. (E) US tracking of an acoustically actuated microswimmer. (e1)–(e3) demonstrate three different events of navigation [68]. Reproduced with permission. Copyright 2019, IEEE.**

the blood clot. After reaching the clot region, thrombolysis process was conducted via the mechanical rubbing between the robot and the clot (Fig. 1(C)). Results showed that the removal rate of mechanical rubbing (-0.56 ± 0.27 mm^3/min) is approximately three times faster than the dissolution rate of pure chemical lysis (-0.17 ± 0.032 mm^3/min) [73]. The rigid structure of a microrobot may cause critical issues when performing tasks in a living body, especially in a confined environment. Soft robot offers more possibility to non-invasively access narrowed, enclosed spaces [74]. In the work proposed by Sitti and co-workers, a miniature soft robot with multimodal locomotion can be *ex vivo* visualized (Fig. 1(D)) [67]. The size of the robot is 3.7 mm $\times$ 185 μm $\times$ 1.5 mm (Length $\times$ Height $\times$ Width). Further scaling down this miniature robot could increase the possibility for medical applications. Besides the passive deformation, adaptive locomotion of soft microrobot has also been proposed [75]. The structural and magnetic properties of the microrobot with the dynamic properties of the surrounding fluid leads to adaptive locomotion. Recently, 4D printing technique shows great potential for fabrication stimuli-responsive soft microrobot [76]–[79]. The microrobots fabricated by smart materials open a new direction for US imaging-guided microrobotics. The imaging contrast can be affected and even tuned by deforming the structure of the microrobot, which benefits the tracking algorithm in recognizing the microrobot from surrounding environments. Moreover, the multi-stimuli response materials offer microrobots the capabilities of biosensing and targeted delivery [80], [81]. The changing of properties in tissues or bio-fluids led to the deformation of a microrobot, which can be detected by US imaging system.

To track a microrobot in multiple planes or three-dimensional (3-D) space, multiple US probes can be applied to acquire images from different focus planes. In a recent work proposed by Chen *et al.*, the position of a 2-D navigated microrobot was tracked using two probes [68]. The 1-D US array probe provides only a cross-sectional image along the US beam direction (axial-lateral coordinates), therefore, two US probes are used to complement each other for capturing the full two-dimensional (2-D) motion of the microrobot that moves along the bottom surface of the tank. This multiple-probe approach demonstrated low tracking error and can be applied to 3-D navigation of untethered objects [82].

B. ULTRASOUND IMAGING OF MICROROBOT WITH BUBBLE-ENHANCED CONTRAST

Bubble-based contrast agents are widely used in clinic and medical imaging systems. These contrast agents used for bubble-enhanced US are microbubbles or gas-filled microparticles, typically with 1–8 μm in diameter [83]. Affected by

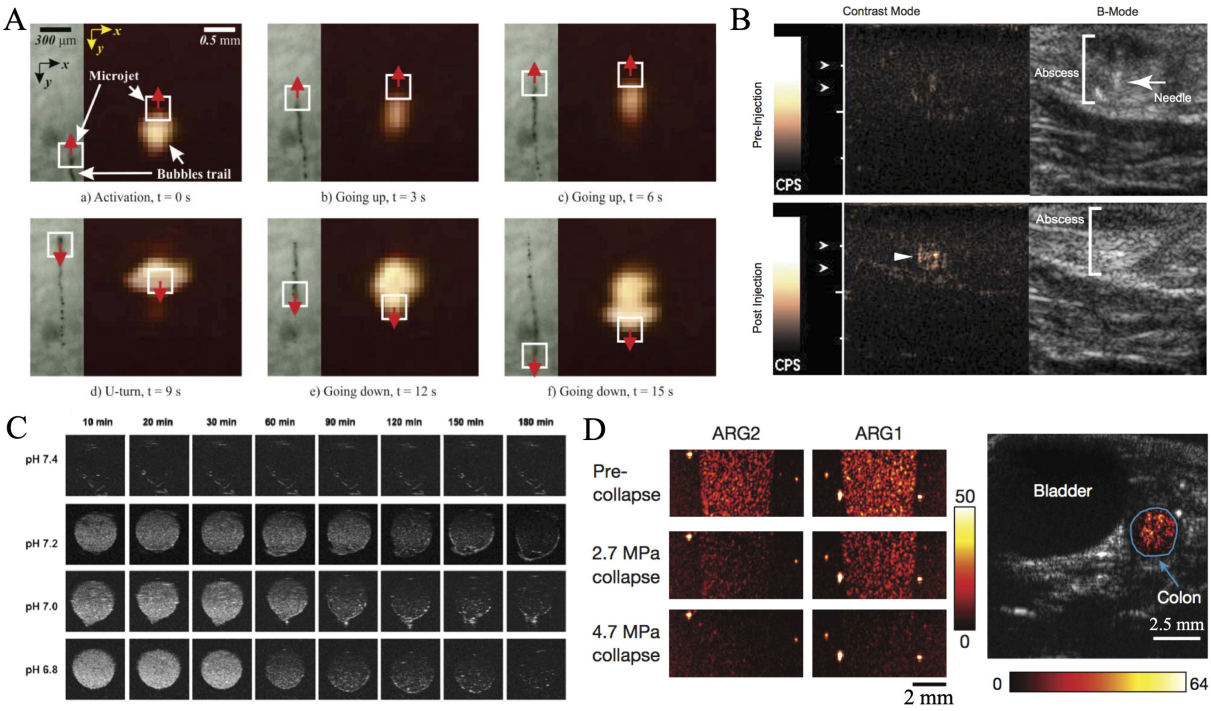

FIGURE 2. **Bubble-enhanced US imaging (contrast-enhanced US). (A) Magnetic control of a bubble-driven magnetic microrobot under US guidance [69]. Reproduced with permission. Copyright 2014, IEEE. (B) NSCs injected at the abscess margin (depicted in orange brackets) results in a discernable increase in signal on contrast mode US (bottom panel, yellow arrowhead) [70]. Reproduced with permission. Copyright 2013, Elsevier. (C) *In vitro* US images of DOX-$CaCO_3$-MNPs in various pH environments [71]. Reproduced with permission. Copyright 2015, American Chemical Society. (D) Left: US images of gel phantoms containing arg1 or arg2 before collapse, after collapse at 2.7 MPa and 4.7 MPa (109 cells ml^{-1}), respectively. Right: US contrast within the colon region of interest [72]. Reproduced with permission. Copyright 2018, Springer Nature.**

the pressure of US waves, microbubbles undergo volume oscillations. They vibrate, resonate, and reemit sound, resulting in the detectable backscattered US signal. The signal can be orders of magnitude stronger than the backscatter of blood, tissues, and organs. This is due to the high acoustic impedance mismatch between gases and blood or soft tissue [84].

Bubble-driven microjets, as one of the chemical-driven microrobots, exhibit motion via thrust force generated by chemical fuel [85], [86]. A typical bubble-driven device use H_2O_2 as the chemical fuel and Pt as the catalyst. Propulsion is achieved due to the catalysis of H_2O_2 by the platinum component of the microrobot, resulting in the ejection of oxygen microbubbles from one of its ends [87]. The generated microbubbles enable the position tracking of the microrobot indirectly. Such method has been proposed by Sanchez *et al.*, where the microrobot was tracked indirectly by employing the strong US contrast of the ejected microbubbles (Fig. 2(A)) [69]. The length and diameter of the microrobot are around 50 μm and 10 μm. Objects with such small size are hard to be directly tracked using typical clinic US system. However, by applying this indirect tracking method, the microrobot was closed-loop controlled to follow two trajectories (diamond shape and figure-eight shape) with an average velocity of 156 ± 35.1 μm/s and tracking error of 250.7 ± 164.7 μm. Much deeper and more meticulous work on US detection of microrobots-produced microbubble was proposed by Olson *et al.* [70]. These microrobots were designed for the detection of H_2O_2, and the influence of concentration of H_2O_2 to the microrobots were experimentally investigated. Results showed that the microbubble production signal can be detected when the microrobots were injected in abscesses, indicating that the elevated levels of H_2O_2 are required (Fig. 2(B)). These *in vivo* experiments showed the potential for biomedicine and biosensing applications by integration microrobotic technique and medical imaging.

In recent years, theranostic nanoparticles, which integrate imaging and therapeutic functionalities, have shown their effectiveness for imaging-guided tumor treatment. For example, doxorubicin-loaded calcium carbonate hybrid nanoparticles (DOX-$CaCO_3$-MNPs) produced carbon dioxide (CO_2) microbubbles at the PH value of tumor acid [71]. Under US imaging, the generated microbubbles were sufficient for echogenic reflectivity. Taking advantage of the multilayer design, the tumor cells were detected and DOX was released to achieve antitumor therapeutic activity (Fig. 2(C)). The fabricated poly(lactic-co-glycolic acid) (PLGA) nanocapsules (perfluorohexane (PFH)@PLGA/Fe_3O_4) can be used to increase the local tumor temperature by absorbing the NIR energy and enhance the bimodal US contrast. By absorbing NIR irradiation, the produced microbubbles were used as the US contrast agent [88]. The proposed approaches inspire the design and imaging of microrobot. By improving

the structure and materials of a microrobot, it can be further used for therapeutic applications with real-time US imaging feedback. Besides the artificial micro- /nano-agents, biohybrid micro- /nano system provides a more complex functionality with biocompatibility [89]. Acoustic reporter genes (ARGs) were recently introduced, which are genetic constructs that allow bacterial gene expression to be visualized *in vivo* using US [72], [90]. These constructs are based on gas vesicles, a unique class of gas-filled protein nanostructures that have the size similar to microbubbles and are capable of enhancing US contrast. Shapiro and co-workers demonstrated that the US imaging of such genetically engineered reporter variants can be tuned by breaking the nanostructure using US wave pressure. The *in vivo* experiments demonstrated that the microorganisms with ARGs were imaged at a resolution of less than 100 μm (Fig. 2(D)). Such genetic approach has the potential to be integrated with micro/nanorobot technology. Combining the controllability of microrobot and the deep US imaging of the ARGs-modified microorganisms, a hybrid microrobot has the potential to be applied in hard-to-reach and deep-tissue environments with promising actuation and imaging ability.

Alternatively, microbubbles can also be produced by using acoustic-driven microrobot. Ahmed *et al.* designed a hybrid acousto-magnetic soft microrobot consisting of a microbubble trapped in a superparamagnetic polymer composite [91]. The soft microrobot contains microcavities at the center of its body. The microcavity supports an air bubble trap, and the trapped microbubble enables propulsion in an external acoustic field. Moreover, acoustically powered microrobots showed swimming on three-dimensional boundaries with single-particle manipulation ability [17]. These microrobots do not need special chemical environments to produce microbubbles, showing a great potential for applications in varied environments. The combination of US for both propulsion and bubble-enhanced imaging shows great research opportunity, whereas challenge remains in the integration of control and imaging systems.

C. ULTRASOUND IMAGING OF SWARMING MICRO/NANOROBOTS

One major challenge of using US imaging to track microrobots is the trade-off between the microrobot size and imaging depth. A large (cm/mm scale) microrobot provides better imaging contrast and drug-loading ability when performing targeted delivery interventions. However, a large-size microrobot limits the application in confined environments, and may cause a critical damage to surrounding tissues. To tackle these issues, a collective of micro/nanorobots shows great potential to be applied in an imaging-guided system. The interactions between building blocks yield various dynamic pattern (e.g., stars [97], disks [98], rings [99], and carpets [100]), which showed controlled assembly and pattern transformation under external energy inputs [101]–[103]. The usage of swarming microrobots for the enhancement of US contrast has shown promising and effective applications. Wang *et al.* demonstrated the US imaging of a paramagnetic nanoparticle-based microswarm [92]. Under a rotating magnetic field, nanoparticle chains were formed and the hydrodynamic interaction among them yielded a region with a high area density of nanoparticles (4–5 μg/mm^2). The backscattered waves were significantly affected by the orientation of the chains inside the microswarm (Fig. 3(A)). The backscattered US waves were increased to the maximum value if the chains were perpendicular to the wave propagation direction ($\alpha = 0^\circ$), which yields the highest contrast. Whereas the contrast decreased by increasing α, where the contrast reached the minimum value when $\alpha = 90^\circ$. Therefore, the imaging contrast showed a periodic change in an actuation cycle, which is the major difference compared to the imaging of an individual microrobot. Such dynamic contrast can be exploited in image processing to improve the signal-to-noise ratio. For example, the image differencing-based processing will eliminate static noise signals and provides a better US contrast for the microswarm, which has been used for real-time feedback control *ex vivo* [93] and proof-of-concept study of imaging-guided thrombolysis [104]. Moreover, the imaging contrast can be enhanced due to the high area density of nanoparticles (Fig. 3(B)). Compare to loosely distributed nanoparticles, the microswarm is able to be localized in deep-tissue site. From clinical aspects, the therapeutic dose of nanoparticles can be further reduced by utilizing this swarming behavior to avoid dose-related toxicity.

Guided by US imaging, the circular-pattern microswarm has been applied in bio-fluids. Bio-fluids contain complex components, in which the viscosity, ionic strengths, and mesh-like structures influence the generation and locomotion of the microswarm. Yu and co-workers demonstrated the strong fluidic forces generated by the rotating microswarm were capable of pushing and twisting the meshes in vitreous humor (Fig. 3(C)). The microswarm was generated, navigated to follow a right-angled path and localized using B-mode US feedback. *Ex vivo* experiments showed swarming generation and navigated locomotion in bovine eyeballs, where initial position of the microswarm was located by observing the syringe needle for injection (Fig. 3(D)). It is noted that the volume of the nanoparticle suspension injected into the bovine eyeball was approximately 0.2 mL, which is a small value compared with the volume of the vitreous humor ($\sim$5 mL). The rotating microswarm also showed locomotion at a speed $\sim$50 μm/s in blood (Fig. 3(E)). These *ex vivo* demonstrations validated the effective application of nanoparticle-based microswarm in various bio-environments, in which the high US contrast enables the real-time imaging and tracking of the microswarm. In addition to the gathering of a microswarm, the area density of nanoparticles is able to be tuned by applying dynamic disassembly fields [95]. The spreading of nanoparticles decreases the area density of nanoparticles in the swarm region, resulting in a weak imaging contrast consequent (Fig. 3(F)). Such process also demonstrated the reconfigurable feature of the microswarm. Compared to the relatively weak interactions between helical

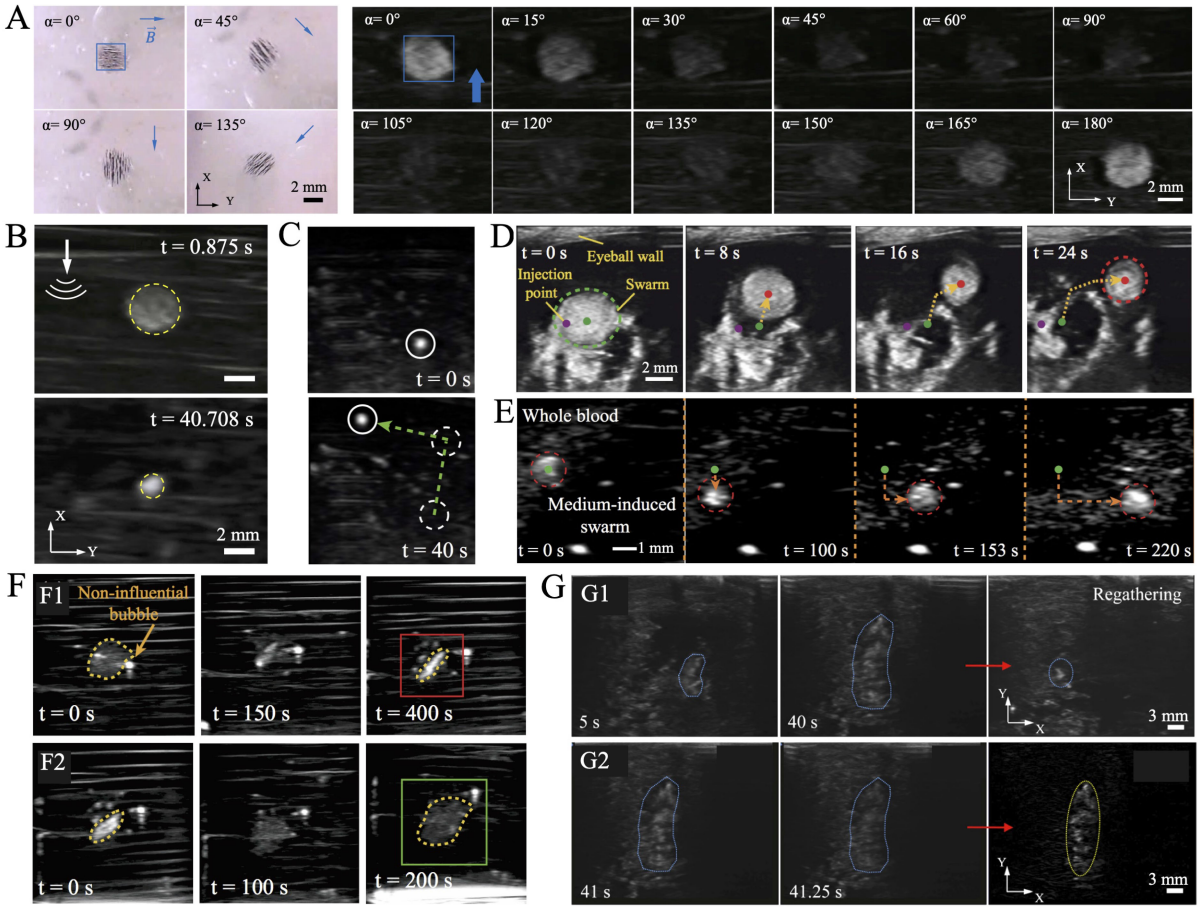

FIGURE 3. **US imaging and tracking of magnetic nanoparticle collectives with the diameter of nanoparticles ranging from 100–500 nm. (A) US imaging of magnetic nanoparticle chains under static magnetic fields. The angle between the US wave propagation direction and the long axis of chains was adjusted [92]. (B) US imaging of the Region of Interest (ROI) before and after forming a microswarm [93]. (A,B) Reproduced with permission. Copyright 2018, IEEE. (C, D, E) Generation and actuation of a vortex-like microswarm in (C) bovine vitreous humor, (D) bovine eyeballs, and (E) blood of mice [94]. (C, D, E) Reproduced with permission. Springer Nature, 2019. (F) Gathering and disassembly of magnetic nanoparticle clusters on a flat surface [95]. Reproduced with permission. Copyright 2019, IEEE. (G) Disassembly and spreading of magnetic nanoparticle clusters on the surface of a swine bladder *ex vivo* [96]. Reproduced with permission. Copyright 2019, Elsevier.**

microrobots [49], the gathering level can be controlled based on the strong interaction between the nanoparticles (e.g., magnetic and hydrodynamic interactions). To further enlarge the application range, US image-guided collective behaviors, such as the gathering and spreading of magnetic nanoparticles, has been performed on uneven surfaces [96]. The disassembly/spreading and gathering process on the surface of a swine bladder *ex vivo* has been demonstrated (Fig. 3(G1)). During actuation, the orientation of nanoparticle chains followed the applied field, i.e., the angle between US wave propagation direction and the particle chains is time-dependent. Therefore, the amount of scattered US waves changes, resulting in a periodic changing of US contrast (Fig. 3(G2)). Thus, the background noise signals were eliminated by image differencing-based processing, and the coverage area was tracked in real-time (the yellow ellipse in Fig. 3(G1)). This approach shows the potential for *in vivo* targeted delivery applications, such as targeted energy delivery (e.g., magnetic hyperthermia). A microswarm pattern has been navigated to the desired location, and the coverage area (area density) was adjusted to satisfy the requirement of both dose (energy density) and region of influence [108]. Such disassembly-regathering behavior can also be induced using acoustic waves [109], which showed a great potential of integrating US for both actuation and imaging of a collective of tiny objects.

Besides US imaging, swarming micro/nanorobots also benefit other imaging systems, such as MRI [110], PA imaging [49], [50], and PET/CT [111]. Unlike the usage of a centimeter or millimeter-scale robot, the generated microswarm is capable of disassembly and regathering to perform cooperative motion. The building blocks can be injected into a confined environment, navigated to the desired location and regathered again to perform demanded diagnostics under varied imaging system.

D. ULTRASOUND DOPPLER IMAGING IN MICROROBOTICS

The fundamental mechanism of the Doppler mode is the Doppler effect, which shows how the frequency of emitted

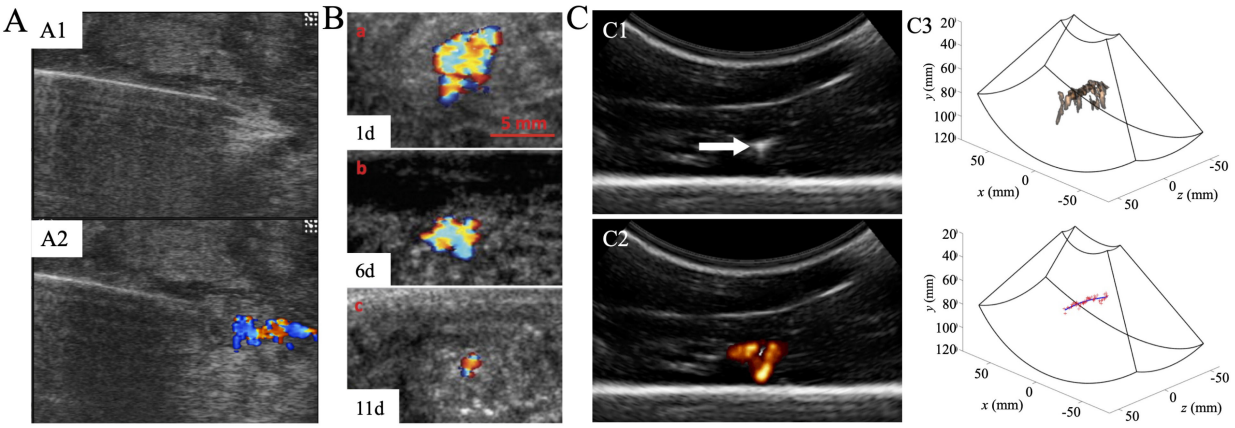

FIGURE 4. **US Doppler imaging in microrobotics. (A) US image of a fresh chicken breast tissue (A1) before and (A2) after injecting hairbots suspension. Color Doppler images showed the speed of the moving hairbots [105]. Reproduced with permission. Copyright 2019, Elsevier. (B) Color Doppler imaging (1, 6, and 11 days after injection) of the nanoshell that injected intratumorally into VX2 tumor-bearing rabbits [106]. Reproduced with permission. Copyright 2015, Wiley. (C) Two-dimensional US images taken from volumetric sweeps of steerable needles inserted into liver *ex vivo:* (C1) B-mode US image; (C2) power Doppler US image captured during needle vibration. (C3) shows the segmentation of needle using Doppler feedback [107]. Reproduced with permission. Copyright 2014, IEEE.**

waves changes with the velocity of the emitter (US probe) or observer (RBCs). A typical clinical application is the quick measurement of blood flow by detecting the motion of red blood cells (RBCs) [112]. RBCs scatter weak US echoes that can be detected by US probes, the temporal shifts observed in consecutive RBC echoes allow detection of the displacement of RBCs and derivation of a Doppler signal proportional to RBC velocity. To date, two Doppler imaging modes are widely used in clinics: color Doppler and power Doppler, which display the velocity and the energy of RBC echoes in vascular system, respectively. Doppler modes are different from the typical B-mode US imaging, which relies on the amplitude of the backscattered US waves. Therefore, Doppler US is a powerful tool to track microrobots in dynamic environments, such as blood vascular system.

Recently, Sitti and co-works proposed hairbots that showed potential as ultrasonography contrast agents [105]. The hairbot was produced using hair as the materials. Superparamagnetic iron oxide nanoparticles were loaded into the hairbots to acquire the responsive to magnetic fields and gradients. The hollow medullary space in the hair provides the possibility of using hairbots as US contrast agents. In the color Doppler mode, the moving hairbots (diameter: $\sim$50 μm) were imaged as dots, where the displayed color depends on the speed of their movement (Fig. 4(A)). In standard B-mode, the hairbots also can be detected. However, the color marked in the Doppler mode separated the hairbots from background tissues. Such color signal can be applied to benefit the following tracking algorithm. Down to nanoscale, functionalized nanoparticles were used as Doppler agents under external stimuli. Among them, the perfluoropentane (PFP) gas-filled silica nanoshells have been demonstrated as long-lived US contrast agents. These agents were typically synthesized by encapsulating a perfluorocarbon gas within a lipid or polymeric shell to produce elastic microbubbles in the range 1–6 μm in diameter. When insonated, these microbubbles oscillate to produce signals at harmonic frequencies and break or collapse into smaller bubbles to produce a broadband signal [113]. As proposed by Liberman *et al.*, the hollow silica nanoshells can be detected *in vivo* using color Doppler imaging with great lifetimes over than 11 days (Fig. 4(B)) [106]. Such functionalized nano-agents can be integrated with the micro/nanorobotics technology to acquire controllable navigation under real-time US Doppler feedback.

Besides the untethered system, recent studies on the Doppler imaging of tethered system showed inspiring results. Vibrating solid objects have been used to produce recognizable Doppler signals in tissue [114]. This concept has been applied to localize straight needles [115], needle tips [116], and instruments in cardiac interventions [117], [118]. Okamura and co-workers demonstrated that high-frequency vibrated needle can be real-time steered under the feedback of 3-D power Doppler imaging [107]. The Doppler response around the needle was produced by vibrating the needle, where a 3-D Doppler image was obtained by sweeping the 2-D scanning plane. The needle shape was reconstructed based on the fit through the centroids of the Doppler data in each image (Fig. 4(C)). The proposed method expanded the Doppler signal from the blood vascular system. For untethered microrobots, the similar mechanism can be applied to introduce Doppler signals in tissues. For example, the vibration of magnetic agents can be introduced using oscillating magnetic fields [119]. These studies indicate that US Doppler imaging detects not only the microrobot itself, but also the affected region by an actuated microrobot (e.g., surrounding tissues, surrounding RBCs). The integration of US Doppler and micro/nanorobotic technology has great potential in medical diagnosis to accurately track and real-time control objects that the typical B-mode hard to provide.

TABLE 1. Summary and Comparison of US Imaging-Guided Micro/Nanorobots for *in Vivo* Applications

US imaging modes	Imaging objects	Advantages	Limitations
B-Mode	Individual milli-/microrobot (e.g., Fig. 1)	♦ Easy to be localized and control; ♦ 3-D actuation and imaging.	♦ Limited applications in confined environments; ♦ Size of an individual microrobot challenges the imaging resolution.
	Microrobots with bubble-enhanced contrast (e.g., Fig. 2)	♦ High signal-to-noise ratio; ♦ Enhanced imaging contrast; ♦ Easy to be localized directly and indirectly.	♦ Limited application environment; ♦ Hard to maintain the stability of microbubble.
	Swarming micro/nanorobots (e.g., Fig. 3)	♦ Dynamic imaging contrast; ♦ Enhanced contrast; ♦ Adaptability to environment; ♦ Controllable behavior for imaging.	♦ Require effective swarm control; ♦ Hard to maintain a high access rate of building blocks.
Doppler Modes	Micro/nanorobots; Swarming micro/nanorobots (e.g., Fig. 4)	♦ High signal-to-noise ratio; ♦ Adjustable sensitivity; ♦ Easy to distinguish from surrounding environments; ♦ Various imaging mode (e.g., color / power / pulse wave Doppler).	♦ Require stable Doppler signal; ♦ Easy to be affected by external disturbances.

III. SUMMARY AND PERSPECTIVES

Untethered micro/nanorobots have been developed to perform demanded biomedical tasks: from targeted delivery, biosensing to minimally invasive surgery and biopsy. In the hard-to-reach place of a living body, they have demonstrated the ability to perform diagnostics and intervention that tethered instruments are hard to achieve. The challenge of *in vivo* imaging remains crucial to allow doctors and medical practitioners to real-time track these small-scale agents in dynamic and complex environments. Therefore, the integration of micro/nanorobotics and medical imaging technologies is urgently required to precisely control these tiny machines under the feedback of imaging system [120].

In this mini-review, we focus on the imaging and tracking of US imaging-guided micro/nanorobots. The advantages and limitations of US imaging-guided micro/nanorobots for *in vivo* applications using different imaging modes are summarized in Table 1. Currently, the B-mode imaging is widely used for imaging robots ranging from centimeter to hundreds of micrometer. However, the usage of a centimeter-/millimeter-scale robot limits the applications in confined, narrowed lumen (e.g., blood vascular system,bile duct), whereas tracking a micrometer-scale microrobot challenges the resolution of US imaging. Deformable soft microrobots fabricated by smart, soft materials (e.g., stimuli-responsive hydrogel) are able to affect imaging contrast by structural changing, which can be recognized from static contrast of environment (e.g., tissue). Microbubble, as a widely-used imaging contrast agent in clinic, shows a promising function when integrating with microrobots. Microrobots with bubble-enhanced contrast have been applied to improve the signal-to-noise ratio. However, the bubble-driven microrobot requires special working environments or actuation methods. US imaging of swarming micro/nanorobots exhibits controllable and dynamic contrast. Although microswarm requires superior swarm control schemes (e.g., pattern navigation), the gathering ability offers them the adaptability to narrowed environments with complex bio-mechanical forces (e.g., pulsating blood flow, body motion). Besides the B-mode imaging, US Doppler imaging provides a new approach for imaging micro/nanorobots. Various Doppler image modes are able to be applied with adjustable sensitivity, and the fast imaging speed is suitable for tracking robots in dynamic environments. Unlike B-mode imaging, Doppler signal highlights not only the micro/nanorobots themselves but also the affected region by the actuated robots. Therefore, the feedback provided by Doppler signal can be treated as an indirect imaging and tracking approach. Swarming micro/nanorobots also offer great possibility in enlarging the affected region. The assembled pattern may affect the surrounding environment that an individual microrobot is hard to perform. The integration of swarming micro/nanorobots with Doppler imaging feedback is worth investigation, especially in a region that B-mode imaging fails to provide enough contrast for tracking the moving micro-/nano-agents.

In the future, the major challenges on applying micro/nanorobots to *in vivo* environments remains in the integration of US imaging system and real-time control system (Fig. 5). The design of micro/nanorobots should satisfy both imaging and application requirements, and actuation methods must be harmless to the living body, such as magnetic actuation at suitable field strengths. Different US imaging modes should be selected according to the specific microrobot or swarming micro/nanorobots, task, and application scenario. The US feedback-based control scheme should take the internal biomechanical forces and external disturbances into consideration. Swarm control will further improve both the adaptability of micro/nanorobots to the surrounding environments and the effectiveness of imaging/tracking. Although real-time formation and navigation of collective micro/nanorobots

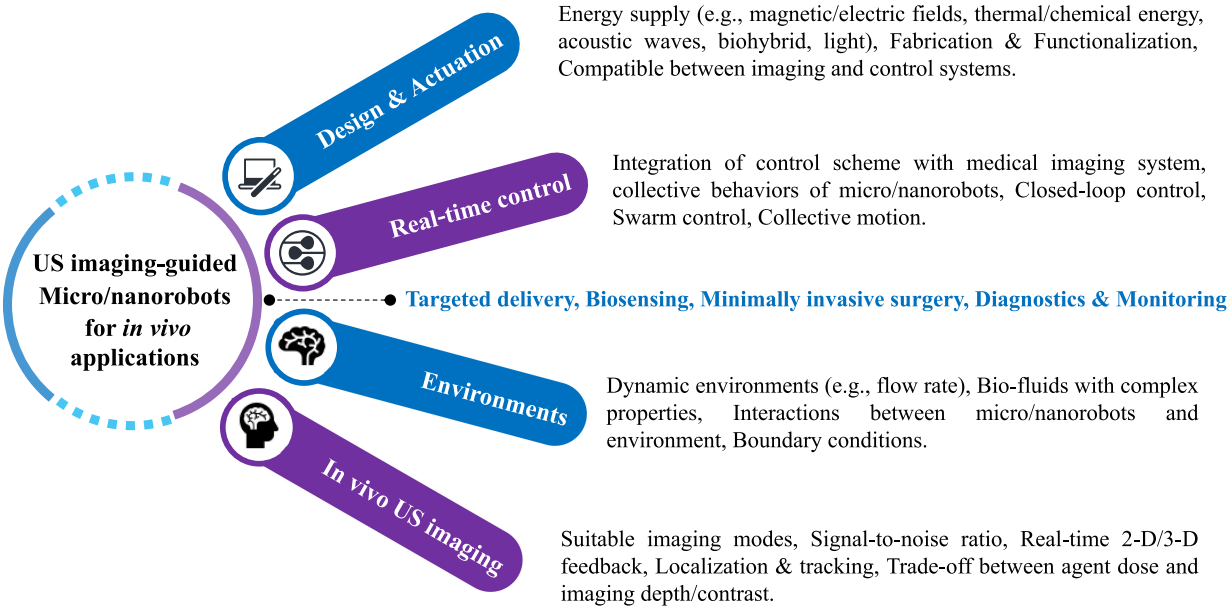

FIGURE 5. **Challenges of real-time imaging and tracking of US imaging-guided micro/nanorobots towards *in vivo* biomedical applications.**

under 3-D US feedback remain challenge, it is a promising approach to conduct targeted delivery tasks. Efforts also be dedicated to the development of feasible testing phantom before conducting *in vivo* trials.

REFERENCES

[1] M. Sitti and D. S. Wiersma, "Pros and cons: Magnetic versus optical microrobots," *Adv. Mater.*, pp. 1–9, doi: 10.1002/adma.201906766.

[2] Y. Kim, H. Yuk, R. Zhao, S. A. Chester, and X. Zhao, "Printing ferromagnetic domains for untethered fast-transforming soft materials," *Nature*, vol. 558, no. 7709, pp. 274–279, 2018.

[3] A. Barbot, H. Tan, M. Power, F. Seichepine, and G.-Z. Yang, "Floating magnetic microrobots for fiber functionalization," *Sci. Robot.*, vol. 4, no. 34, 2019, Art. no. eaax8336.

[4] T. Xu, J. Zhang, M. Salehizadeh, O. Onaizah, and E. Diller, "Millimeter-scale flexible robots with programmable three-dimensional magnetization and motions," *Sci. Robot.*, vol. 4, no. 29, 2019, Art. no. eaav4494.

[5] S. Shahrokhi, J. Shi, B. Isichei, and A. T. Becker, "Exploiting nonslip wall contacts to position two particles using the same control input," *IEEE Trans. Robot.*, vol. 35, no. 3, pp. 577–588, Jun. 2019.

[6] L. Zhang, J. J. Abbott, L. Dong, B. E. Kratochvil, D. Bell, and B. J. Nelson, "Artificial bacterial flagella: Fabrication and magnetic control," *Appl. Phys. Lett.*, vol. 94, no. 6, 2009, Art. no. 064107.

[7] X.-Z. Chen *et al.*, "Small-scale machines driven by external power sources," *Adv. Mater.*, vol. 30, no. 15, 2018, Art. no. 1705061.

[8] L. Yang, Q. Wang, and L. Zhang, "Model-free trajectory tracking control of two-particle magnetic microrobot," *IEEE Trans. Nanotechnol.*, vol. 17, no. 4, pp. 697–700, Jul. 2018.

[9] B. Chaluvadi, K. M. Stewart, A. J. Sperry, H. C. Fu, and J. J. Abbott, "Kinematic model of a magnetic-microrobot swarm in a rotating magnetic dipole field," *IEEE Robot. Automat. Lett.*, vol. 5, no. 2, pp. 2419–2426, Apr. 2020.

[10] L. Kong, C. C. Mayorga-Martinez, J. Guan, and M. Pumera, "Photocatalytic micromotors activated by UV to visible light for environmental remediation, micropumps, reversible assembly, transportation, and biomimicry," *Small*, pp. 1–14, doi: 10.1002/smll.201903179.

[11] S. Tottori, L. Zhang, F. Qiu, K. K. Krawczyk, A. Franco-Obregón, and B. J. Nelson, "Magnetic helical micromachines: Fabrication, controlled swimming, and cargo transport," *Adv. Mater.*, vol. 24, no. 6, pp. 811–816, 2012.

[12] I. S. M. Khalil, V. Magdanz, S. Sanchez, O. G. Schmidt, and S. Misra, "The control of self-propelled microjets inside a microchannel with time-varying flow rates," *IEEE Trans. Robot.*, vol. 30, no. 1, pp. 49–58, Feb. 2014.

[13] W. Gao *et al.*, "Artificial micromotors in the mouse's stomach: A step toward in vivo use of synthetic motors," *ACS Nano*, vol. 9, no. 1, pp. 117–123, 2015.

[14] J. Katuri, X. Ma, M. M. Stanton, and S. Sanchez, "Designing micro- and nanoswimmers for specific applications," *Accounts Chem. Res.*, vol. 50, no. 1, pp. 2–11, 2017.

[15] D. Xu, Y. Wang, C. Liang, Y. You, S. Sanchez, and X. Ma, "Self-propelled micro/nanomotors for on-demand biomedical cargo transportation," *Small*, pp. 1–22, doi: 10.1002/smll.201902464.

[16] X. Lin, Z. Wu, Y. Wu, M. Xuan, and Q. He, "Self-propelled micro-/nanomotors based on controlled assembled architectures," *Adv. Mater.*, vol. 28, no. 6, pp. 1060–1072, 2016.

[17] L. Ren *et al.*, "3D steerable, acoustically powered microswimmers for single-particle manipulation," *Sci. Adv.*, vol. 5, no. 10, 2019, Art. no. eaax3084.

[18] Y. Alapan *et al.*, "Soft erythrocyte-based bacterial microswimmers for cargo delivery," *Sci. Robot.*, vol. 3, no. 17, 2018, Art. no. eaar4423.

[19] L. Schwarz, M. Medina-Sánchez, and O. G. Schmidt, "Hybrid biomicromotors," *Appl. Phys. Rev.*, vol. 4, no. 3, 2017, Art. no. 031301.

[20] K. Bente, A. Codutti, F. Bachmann, and D. Faivre, "Biohybrid and bioinspired magnetic microswimmers," *Small*, vol. 14, no. 29, 2018, Art. no. 1704374.

[21] D. Loghin, C. Tremblay, M. Mohammadi, and S. Martel, "Exploiting the responses of magnetotactic bacteria robotic agents to enhance displacement control and swarm formation for drug delivery platforms," *Int. J. Robot. Res.*, vol. 36, no. 11, pp. 1195–1210, 2017.

[22] L. Ricotti *et al.*, "Biohybrid actuators for robotics: A review of devices actuated by living cells," *Sci. Robot.*, vol. 2, no. 12, 2017, Art. no. eaaq0495.

[23] M. Medina-Sánchez, L. Schwarz, A. K. Meyer, F. Hebenstreit, and O. G. Schmidt, "Cellular cargo delivery: Toward assisted fertilization by sperm-carrying micromotors," *Nano Lett.*, vol. 16, no. 1, pp. 555–561, 2016.

[24] C. Zhang, J. Wang, W. Wang, N. Xi, Y. Wang, and L. Liu, "Modeling and analysis of bio-syncretic micro-swimmers for cardiomyocyte-based actuation," *Bioinspiration Biomimetics*, vol. 11, no. 5, 2016, Art. no. 056006.

[25] G.-Z. Yang *et al.*, "The grand challenges of science robotics," *Sci. Robot.*, vol. 3, no. 14, 2018, Art. no. eaar7650.

[26] M. Sitti, "Miniature soft robots–road to the clinic," *Nature Rev. Mater.*, vol. 3, no. 6, pp. 74–75, 2018.

[27] R. D. Field, P. N. Anandakumaran, and S. K. Sia, "Soft medical microrobots: Design components and system integration," *Appl. Phys. Rev.*, vol. 6, no. 4, 2019, Art. no. 041305.

[28] J. Ou *et al.*, "Micro-/nanomotors toward biomedical applications: The recent progress in biocompatibility," *Small*, pp. 1–16, doi: 10.1002/smll.201906184.

[29] H. Ceylan, J. Giltinan, K. Kozielski, and M. Sitti, "Mobile microrobots for bioengineering applications," *Lab Chip*, vol. 17, no. 10, pp. 1705–1724, 2017.

[30] B. J. Nelson, I. K. Kaliakatsos, and J. J. Abbott, "Microrobots for minimally invasive medicine," *Annu. Rev. Biomed. Eng.*, vol. 12, pp. 55–85, 2010.

[31] M. Sitti *et al.*, "Biomedical applications of untethered mobile milli/microrobots," *Proc. IEEE*, vol. 103, no. 2, pp. 205–224, Feb. 2015.

[32] S. C. Lenaghan *et al.*, "Grand challenges in bioengineered nanorobotics for cancer therapy," *IEEE Trans. Biomed. Eng.*, vol. 60, no. 3, pp. 667–673, Mar. 2013.

[33] J. Yu, B. Wang, X. Du, Q. Wang, and L. Zhang, "Ultra-extensible ribbon-like magnetic microswarm," *Nature Commun.*, vol. 9, no. 1, 2018, Art. no. 3260.

[34] Z. Wu *et al.*, "A swarm of slippery micropropellers penetrates the vitreous body of the eye," *Sci. Adv.*, vol. 4, no. 11, 2018, Art. no. eaat4388.

[35] L. Yang, Y. Zhang, Q. Wang, K.-F. Chan, and L. Zhang, "Automated control of magnetic spore-based microrobot using fluorescence imaging for targeted delivery with cellular resolution," *IEEE Trans. Automat. Sci. Eng.*, vol. 17, no. 1, pp. 490–501, Jan. 2020.

[36] J. Li *et al.*, "Development of a magnetic microrobot for carrying and delivering targeted cells," *Sci. Robot.*, vol. 3, no. 19, 2018, Art. no. eaat8829.

[37] Y. Zhang *et al.*, "Real-time tracking of fluorescent magnetic spore–based microrobots for remote detection of c. diff toxins," *Sci. Adv.*, vol. 5, no. 1, 2019, Art. no. eaau9650.

[38] J. Li, B. E.-F. de Avila, W. Gao, L. Zhang, and J. Wang, "Micro/nanorobots for biomedicine: Delivery, surgery, sensing, and detoxification," *Sci. Robot.*, vol. 2, no. 4, 2017, Art. no. eaam6431.

[39] B. Esteban-Fernandez de Avila *et al.*, "Aptamer-modified graphene-based catalytic micromotors: Off–on fluorescent detection of ricin," *ACS Sensors*, vol. 1, no. 3, pp. 217–221, 2016.

[40] Á. Molinero-Fernández, A. Jodra, M. Moreno-Guzmán, M. Á. López, and A. Escarpa, "Magnetic reduced graphene oxide/nickel/platinum nanoparticles micromotors for mycotoxin analysis," *Chemistry–A Eur. J.*, vol. 24, no. 28, pp. 7172–7176, 2018.

[41] L. Yang, Y. Zhang, Q. Wang, and L. Zhang, "An automated microrobotic platform for rapid detection of c. diff toxins," *IEEE Trans. Biomed. Eng.*, vol. 67, no. 5, pp. 1517–1527, May 2020.

[42] E. B. Steager, M. S. Sakar, C. Magee, M. Kennedy, A. Cowley, and V. Kumar, "Automated biomanipulation of single cells using magnetic microrobots," *Int. J. Robot. Res.*, vol. 32, no. 3, pp. 346–359, 2013.

[43] C. Pacchierotti *et al.*, "Steering and control of miniaturized untethered soft magnetic grippers with haptic assistance," *IEEE Trans. Automat. Sci. Eng.*, vol. 15, no. 1, pp. 290–306, Jan. 2018.

[44] W. Jing *et al.*, "A microforce-sensing mobile microrobot for automated micromanipulation tasks," *IEEE Trans. Automat. Sci. Eng.*, vol. 16, no. 2, pp. 518–530, Apr. 2019.

[45] M. P. Kummer, J. J. Abbott, B. E. Kratochvil, R. Borer, A. Sengul, and B. J. Nelson, "Octomag: An electromagnetic system for 5-DoF wireless micromanipulation," *IEEE Trans. Robot.*, vol. 26, no. 6, pp. 1006–1017, Dec. 2010.

[46] C. Bergeles and G.-Z. Yang, "From passive tool holders to microsurgeons: safer, smaller, smarter surgical robots," *IEEE Trans. Biomed. Eng.*, vol. 61, no. 5, pp. 1565–1576, May 2014.

[47] C. Bergeles, B. E. Kratochvil, and B. J. Nelson, "Visually servoing magnetic intraocular microdevices," *IEEE Trans. Robot.*, vol. 28, no. 4, pp. 798–809, Aug. 2012.

[48] A. W. Mahoney and J. J. Abbott, "Five-degree-of-freedom manipulation of an untethered magnetic device in fluid using a single permanent magnet with application in stomach capsule endoscopy," *Int. J. Robot. Res.*, vol. 35, no. 1-3, pp. 129–147, 2016.

[49] A. Servant, F. Qiu, M. Mazza, K. Kostarelos, and B. J. Nelson, "Controlled in vivo swimming of a swarm of bacteria-like microrobotic flagella," *Adv. Mater.*, vol. 27, no. 19, pp. 2981–2988, 2015.

[50] Z. Wu *et al.*, "A microrobotic system guided by photoacoustic computed tomography for targeted navigation in intestines in vivo," *Sci. Robot.*, vol. 4, no. 32, 2019, Art. no. eaax0613.

[51] F. Peng, Y. Tu, and D. A. Wilson, "Micro/nanomotors towards in vivo application: Cell, tissue and biofluid," *Chem. Soc. Rev.*, vol. 46, no. 17, pp. 5289–5310, 2017.

[52] S. Jeon *et al.*, "Magnetically actuated microrobots as a platform for stem cell transplantation," *Sci. Robot.*, vol. 4, no. 30, 2019, Art. no. eaav4317.

[53] B. Wang, Y. Zhang, and L. Zhang, "Recent progress on micro-and nano-robots: Towards in vivo tracking and localization," *Quantitative Imag. Medicine Surgery*, vol. 8, no. 5, pp. 461–479, 2018.

[54] H. Ceylan, I. C. Yasa, U. Kilic, W. Hu, and M. Sitti, "Translational prospects of untethered medical microrobots," *Prog. Biomed. Eng.*, vol. 1, no. 1, 2019, Art. no. 012002.

[55] S. B. Kesner and R. D. Howe, "Robotic catheter cardiac ablation combining ultrasound guidance and force control," *Int. J. Robot. Res.*, vol. 33, no. 4, pp. 631–644, 2014.

[56] G.-Q. Zhou, W.-W. Jiang, K.-L. Lai, and Y.-P. Zheng, "Automatic measurement of spine curvature on 3-D ultrasound volume projection image with phase features," *IEEE Trans. Med. Imag.*, vol. 36, no. 6, pp. 1250–1262, Jun. 2017.

[57] J. Guo, C. Shi, and H. Ren, "Ultrasound-assisted guidance with force cues for intravascular interventions," *IEEE Trans. Automat. Sci. Eng.*, vol. 16, no. 1, pp. 253–260, Jan. 2019.

[58] Q. François, A. André, B. Duplat, S. Haliyo, and S. Régnier, "Tracking systems for intracranial medical devices: A review," *Med. Devices Sensors*, vol. 2, no. 2, 2019, Art. no. e10033.

[59] J. Zhang, E. Luijten, B. A. Grzybowski, and S. Granick, "Active colloids with collective mobility status and research opportunities," *Chem. Soc. Rev.*, vol. 46, no. 18, pp. 5551–5569, 2017.

[60] G. Kokot and A. Snezhko, "Manipulation of emergent vortices in swarms of magnetic rollers," *Nature Commun.*, vol. 9, no. 1, pp. 1–7, 2018.

[61] C. Liu, T. Xu, L.-P. Xu, and X. Zhang, "Controllable swarming and assembly of micro/nanomachines," *Micromachines*, vol. 9, no. 1, 2018, Art. no. 10.

[62] Z. Lin, C. Gao, M. Chen, X. Lin, and Q. He, "Collective motion and dynamic self-assembly of colloid motors," *Current Opinion Colloid Interface Sci.*, vol. 35, pp. 51–58, 2018.

[63] L. Yang, J. Yu, and L. Zhang, "Statistics-based automated control for a swarm of paramagnetic nanoparticles in 2-D space," *IEEE Trans. Robot.*, vol. 36, no. 1, pp. 254–270, Feb. 2020.

[64] I. S. Khalil, P. Ferreira, R. Eleutério, C. L. de Korte, and S. Misra, "Magnetic-based closed-loop control of paramagnetic microparticles using ultrasound feedback," in *Proc. IEEE Int. Conf. Robot. Automat.*, 2014, pp. 3807–3812.

[65] S. Scheggi *et al.*, "Magnetic motion control and planning of untethered soft grippers using ultrasound image feedback," in *Proc. IEEE Int. Conf. Robot. Automat.*, 2017, pp. 6156–6161.

[66] I. S. Khalil *et al.*, "Mechanical rubbing of blood clots using helical robots under ultrasound guidance," *IEEE Robot. Automat. Lett.*, vol. 3, no. 2, pp. 1112–1119, Apr. 2018.

[67] W. Hu, G. Z. Lum, M. Mastrangeli, and M. Sitti, "Small-scale soft-bodied robot with multimodal locomotion," *Nature*, vol. 554, no. 7690, pp. 81–85, 2018.

[68] Q. Chen, F.-W. Liu, Z. Xiao, N. Sharma, S. K. Cho, and K. Kim, "Ultrasound tracking of the acoustically actuated microswimmer," *IEEE Trans. Biomed. Eng.*, vol. 66, no. 11, pp. 3231–3237, Nov. 2019.

[69] A. Sánchez, V. Magdanz, O. G. Schmidt, and S. Misra, "Magnetic control of self-propelled microjets under ultrasound image guidance," in *Proc. IEEE RAS/EMBS Int. Conf. Biomed. Robot. Biomechatronics.*, 2014, pp. 169–174.

[70] E. S. Olson *et al.*, "Toward in vivo detection of hydrogen peroxide with ultrasound molecular imaging," *Biomaterials*, vol. 34, no. 35, pp. 8918–8924, 2013.

[71] K. H. Min *et al.*, "PH-controlled gas-generating mineralized nanoparticles: A theranostic agent for ultrasound imaging and therapy of cancers," *ACS Nano*, vol. 9, no. 1, pp. 134–145, 2015.

[72] R. W. Bourdeau *et al.*, "Acoustic reporter genes for noninvasive imaging of microorganisms in mammalian hosts," *Nature*, vol. 553, no. 7686, pp. 86–90, 2018.

[73] I. S. Khalil, A. F. Tabak, K. Sadek, D. Mahdy, N. Hamdi, and M. Sitti, "Rubbing against blood clots using helical robots: Modeling and in vitro experimental validation," *IEEE Robot. Automat. Lett.*, vol. 2, no. 2, pp. 927–934, Apr. 2017.

[74] C. Hu, S. Pané, and B. J. Nelson, "Soft micro-and nanorobotics," *Annu. Rev. Control, Robot. Auton. Syst.*, vol. 1, pp. 53–75, 2018.

[75] H.-W. Huang, F. E. Uslu, P. Katsamba, E. Lauga, M. Sakar, and B. Nelson, "Adaptive locomotion of artificial microswimmers," *Sci. Adv.*, vol. 5, no. 1, 2019, Art. no. eaau1532.

[76] D. Jin, Q. Chen, T.-Y. Huang, J. Huang, L. Zhang, and H. Duan, "Four-dimensional direct laser writing of reconfigurable compound micromachines," *Mater. Today*, vol. 32, pp. 19–25, 2020.

[77] D. Martella, S. Nocentini, D. Nuzhdin, C. Parmeggiani, and D. S. Wiersma, "Photonic microhand with autonomous action," *Adv. Mater.*, vol. 29, no. 42, 2017, Art. no. 1704047.

[78] A. Tudor *et al.*, "Fabrication of soft, stimulus-responsive structures with sub-micron resolution via two-photon polymerization of poly (ionic liquid) s," *Mater. Today*, vol. 21, no. 8, pp. 807–816, 2018.

[79] Y. Hu *et al.*, "Botanical-inspired 4d printing of hydrogel at the microscale," *Adv. Funct. Mater.*, vol. 30, no. 4, 2020, Art. no. 1907377.

[80] H. Li, G. Go, S. Y. Ko, J.-O. Park, and S. Park, "Magnetic actuated PH-responsive hydrogel-based soft micro-robot for targeted drug delivery," *Smart Mater. Struct.*, vol. 25, no. 2, 2016, Art. no. 027001.

[81] S. Fusco *et al.*, "An integrated microrobotic platform for on-demand, targeted therapeutic interventions," *Adv. Mater.*, vol. 26, no. 6, pp. 952–957, 2014.

[82] A. Fenster, D. B. Downey, and H. N. Cardinal, "Three-dimensional ultrasound imaging," *Phys. Medicine Biol.*, vol. 46, no. 5, pp. R67–R99, 2001.

[83] S. Unnikrishnan and A. L. Klibanov, "Microbubbles as ultrasound contrast agents for molecular imaging: Preparation and application," *Amer. J. Roentgenol.*, vol. 199, no. 2, pp. 292–299, 2012.

[84] S. Hernot and A. L. Klibanov, "Microbubbles in ultrasound-triggered drug and gene delivery," *Adv. Drug Del. Rev.*, vol. 60, no. 10, pp. 1153–1166, 2008.

[85] A. A. Solovev, Y. Mei, E. B. Ureña, G. Huang, and O. G. Schmidt, "Catalytic microtubular jet engines self-propelled by accumulated gas bubbles," *Small*, vol. 5, no. 14, pp. 1688–1692, 2009.

[86] D. Li, Y. Liu, Y. Yang, and Y. Shen, "A fast and powerful swimming microrobot with a serrated tail enhanced propulsion interface," *Nanoscale*, vol. 10, no. 42, pp. 19673–19677, 2018.

[87] V. M. Fomin, M. Hippler, V. Magdanz, L. Soler, S. Sanchez, and O. G. Schmidt, "Propulsion mechanism of catalytic microjet engines," *IEEE Trans. Robot.*, vol. 30, no. 1, pp. 40–48, Feb. 2014.

[88] Y. Zhao *et al.*, "Phase-shifted pfh@ plga/fe3o4 nanocapsules for mri/us imaging and photothermal therapy with near-infrared irradiation," *ACS Appl. Mater. Interfaces*, vol. 7, no. 26, pp. 14231–14242, 2015.

[89] O. Felfoul *et al.*, "Magneto-aerotactic bacteria deliver drug-containing nanoliposomes to tumour hypoxic regions," *Nature Nanotechnol.*, vol. 11, no. 11, pp. 941–947, 2016.

[90] D. Maresca *et al.*, "Biomolecular ultrasound and sonogenetics," *Annu. Rev. Chem. Biomolecular Eng.*, vol. 2, pp. 229–252, 2018.

[91] D. Ahmed, C. Dillinger, A. Hong, and B. J. Nelson, "Artificial acoustomagnetic soft microswimmers," *Adv. Mater. Technol.*, vol. 2, no. 7, 2017, Art. no. 1700050.

[92] Q. Wang, L. Yang, J. Yu, C.-I. Vong, P. W. Y. Chiu, and L. Zhang, "Magnetic navigation of a rotating colloidal swarm using ultrasound images," in *Proc. IEEE/RSJ Int. Conf. Intell. Robots Syst.*, 2018, pp. 5380–5385.

[93] Q. Wang, L. Yang, J. Yu, P. Chiu, Y.-P. Zheng, and L. Zhang, "Real-time magnetic navigation of a rotating colloidal microswarm under ultrasound guidance," *IEEE Trans. Biomed. Eng.*, 2020, to be published. doi: 10.1109/TBME.2020.2987045.

[94] J. Yu, D. Jin, K.-F. Chan, Q. Wang, K. Yuan, and L. Zhang, "Active generation and magnetic actuation of microrobotic swarms in bio-fluids," *Nature Commun.*, vol. 10, 2019, Art. no. 5631.

[95] J. Yu *et al.*, "Characterizing nanoparticle swarms with tuneable concentrations for enhanced imaging contrast," *IEEE Robot. Automat. Lett.*, vol. 4, no. 3, pp. 2942–2949, Jul. 2019.

[96] Q. Wang, J. Yu, K. Yuan, L. Yang, D. Jin, and L. Zhang, "Disassembly and spreading of magnetic nanoparticle clusters on uneven surfaces," *Appl. Mater. Today*, vol. 18, 2020, Art. no. 100489.

[97] Q. Wang, L. Yang, B. Wang, E. Yu, J. Yu, and L. Zhang, "Collective behavior of reconfigurable magnetic droplets via dynamic self-assembly," *ACS Appl. Mater. Interfaces*, vol. 11, no. 1, pp. 1630–1637, 2019.

[98] P. J. Vach, D. Walker, P. Fischer, P. Fratzl, and D. Faivre, "Pattern formation and collective effects in populations of magnetic microswimmers," *J. Phys. D: Appl. Phys.*, vol. 50, no. 11, 2017, Art. no. 11LT03.

[99] F. Martinez-Pedrero, A. Cebers, and P. Tierno, "Dipolar rings of microscopic ellipsoids: Magnetic manipulation and cell entrapment," *Phys. Rev. Appl.*, vol. 6, no. 3, 2016, Art. no. 034002.

[100] H. Massana-Cid, F. Meng, D. Matsunaga, R. Golestanian, and P. Tierno, "Tunable self-healing of magnetically propelling colloidal carpets," *Nature Commun.*, vol. 10, no. 1, 2019, Art. no. 2444.

[101] A. Snezhko and I. S. Aranson, "Magnetic manipulation of self-assembled colloidal asters," *Nature Mater.*, vol. 10, no. 9, pp. 698–703, 2011.

[102] B. Wang, F. Ji, J. Yu, L. Yang, Q. Wang, and L. Zhang, "Bubble-assisted three-dimensional ensemble of nanomotors for improved catalytic performance," *iScience*, vol. 19, pp. 760–771, 2019.

[103] H. Xie *et al.*, "Reconfigurable magnetic microrobot swarm: Multimode transformation, locomotion, and manipulation," *Sci. Robot.*, vol. 4, no. 28, 2019, Art. no. eaav8006.

[104] Q. Wang, B. Wang, J. Yu, K. Schweizer, B. J. Nelson, and L. Zhang, "Reconfigurable magnetic microswarm for thrombolysis under ultrasound imaging," in *Proc. IEEE Int. Conf. Robot. Automat.*, 2020, to be published.

[105] A. V. Singh *et al.*, "Multifunctional magnetic hairbot for untethered osteogenesis, ultrasound contrast imaging and drug delivery," *Biomaterials*, vol. 219, 2019, Art. no. 119394.

[106] A. Liberman *et al.*, "Mechanically tunable hollow silica ultrathin nanoshells for ultrasound contrast agents," *Adv. Funct. Mater.*, vol. 25, no. 26, pp. 4049–4057, 2015.

[107] T. K. Adebar, A. E. Fletcher, and A. M. Okamura, "3-D ultrasound-guided robotic needle steering in biological tissue," *IEEE Trans. Biomed. Eng.*, vol. 61, no. 12, pp. 2899–2910, Dec. 2014.

[108] B. Wang *et al.*, "Reconfigurable swarms of ferromagnetic colloids for enhanced local hyperthermia," *Adv. Funct. Mater.*, vol. 28, no. 25, 2018, Art. no. 1705701.

[109] T. Xu *et al.*, "Reversible swarming and separation of self-propelled chemically powered nanomotors under acoustic fields," *J. Amer. Chem. Soc.*, vol. 137, no. 6, pp. 2163–2166, 2015.

[110] X. Yan *et al.*, "Multifunctional biohybrid magnetite microrobots for imaging-guided therapy," *Sci. Robot.*, vol. 2, no. 12, 2017, Art. no. eaaq1155.

[111] D. Vilela *et al.*, "Medical imaging for the tracking of micromotors," *ACS Nano*, vol. 12, no. 2, pp. 1220–1227, 2018.

[112] P. R. Hoskins, "Simulation and validation of arterial ultrasound imaging and blood flow," *Ultrasound Medicine Biol.*, vol. 34, no. 5, pp. 693–717, 2008.

[113] C. Sonne *et al.*, "Differences in definity and optison microbubble destruction rates at a similar mechanical index with different real-time perfusion systems," *J. Amer. Soc. Echocardiogr.*, vol. 16, no. 11, pp. 1178–1185, 2003.

[114] J. Holen, R. C. Waag, and R. Gramiak, "Representations of rapidly oscillating structures on the doppler display," *Ultrasound Medicine Biol.*, vol. 11, no. 2, pp. 267–272, 1985.

[115] G. Armstrong *et al.*, "Localization of needle tip with color doppler during pericardiocentesis: In vitro validation and initial clinical application," *J. Amer. Soc. Echocardiogr.*, vol. 14, no. 1, pp. 29–37, 2001.

[116] A. Harmat, R. N. Rohling, and S. E. Salcudean, "Needle tip localization using stylet vibration," *Ultrasound Medicine Biol.*, vol. 32, no. 9, pp. 1339–1348, 2006.

[117] M. P. Fronheiser, S. F. Idriss, P. D. Wolf, and S. W. Smith, "Vibrating interventional device detection using real-time 3-D color Doppler," *IEEE Trans. Ultrasonics, Ferroelectrics, Freq. Control*, vol. 55, no. 6, pp. 1355–1362, Feb. 2008.

[118] K. E. Reddy, E. D. Light, D. J. Rivera, J. A. Kisslo, and S. W. Smith, "Color Doppler imaging of cardiac catheters using vibrating motors," *Ultrason. Imag.*, vol. 30, no. 4, pp. 247–250, 2008.

[119] L. Yang, Q. Wang, C.-I. Vong, and L. Zhang, "A miniature flexible-link magnetic swimming robot with two vibration modes: Design, modeling and characterization," *IEEE Robot. Automat. Lett.*, vol. 2, no. 4, pp. 2024–2031, Oct. 2017.
[120] M. Medina-Sanchez and O. G. Schmidt, "Medical microbots need better imaging and control," *Nature News*, vol. 545, no. 7655, pp. 406–408, 2017.

QIANQIAN WANG (Student Member, IEEE) received the B.Eng. degree from the Hefei University of Technology, Hefei, China, and the M.S. degree from The Hong Kong University of Science and Technology, Hong Kong, China, in 2015 and 2016, respectively, both in mechanical engineering. He is currently working toward the Ph.D. degree with the Department of Mechanical and Automation Engineering, The Chinese University of Hong Kong, Hong Kong, China.

His research interests include magnetic self-assembly, collective behaviors of micro/nanorobots, swarm control, and ultrasound imaging-guided delivery.

LI ZHANG (Senior Member, IEEE) received the Ph.D. degree from the University of Basel, Basel, Switzerland, in 2007. He joined the Institute of Robotics and Intelligent Systems (IRIS), Swiss Federal Institute of Technology (ETH) Zurich, Switzerland, as a Postdoctoral Fellow, in 2007 and as a Senior Scientist from 2009 to 2012. He is currently an Associate Professor in the Department of Mechanical and Automation Engineering, The Chinese University of Hong Kong, Hong Kong, China.

His main research interests include micro- and nanorobotics for biomedical applications and their collective behaviors. Dr. Zhang received the Hong Kong RGC Early Career Award in 2013, and several awards from IEEE conferences, such as ICRA, IROS, and NANOMED. He is appointed by the IEEE NTC as a Distinguished Lecturer for 2020.